

White book on the realization of molecular electrodes and devices fabrication

prepared as: MoQuaS deliverable

updated: 6/10/2016



Outline:

Objectives

- to fix benchmarks for the rate of success in the realization of electrodes and devices at molecular scale
- to evidence critical steps in the fabrication of molecular based devices and propose solutions.

Topics

- metal-based electrodes
- graphene-based electrodes
- electro-migrated junctions
- contacting GNR
- devices combining graphene & molecules.

Methods

- define fabrication procedures
- statistics: evaluate rate of success
- to evidence critical points
- to propose solutions to problems.

Electro-migrated and lithographically defined Nanojunctions

A nanojunction consists of two electrodes which are referred to as source and drain electrode, respectively. Each electrode on a chip can then be divided into two parts: On the one hand it has to have a large area which allows for a connection to the macroscopic world by wire bonding or with a conductive needle which comes from any measurement device. Secondly, as it is meant to contact nanoscopic structures like graphene nanoribbons (GNRs) or magnetic molecules (SMMs), it has to be narrowed down in its width. The actual gap between the electrodes must not be larger than a few nanometers for molecules to fit in, or tens of nanometers for the larger systems, such as graphene nanoribbons or carbon nanotubes (CNTs). Here two options are available: Either the gap is produced by the so-called electro-migration technique or the gap is defined by lithographical means. Nanojunctions can be made either by metals or by graphitic layers as described in the following sections.

Metal-based electrodes: lithographically defined nanojunctions.

This process for the fabrication of metallic nanojunctions starts off with the bare substrate. In the usual case the substrate is a commercially available, degenerately doped silicon wafer. It is covered by a silicon oxide layer of 50 – 300 nm. The advantage of using such substrates is that the conductive silicon may serve as a back gate electrode whilst the silicon oxide forms an insulating back gate barrier. This allows for the application of an electric field and therefore the functionality of a field effect transistor (FET). First, a four inch wafer is cut into smaller pieces with a size of typically 1x1 cm². In a first electron beam lithography step, the actual nanojunction is defined. We optimized the exposure and development parameters such, that even in this step Polymethylmethacrylat (PMMA) as electron beam resist gives a sufficiently high resolution. This is the most common and one of the best value electron beam resists available. Virtually any metal can then be evaporated and used to form the electrodes. That can be good metal, such as gold, platinum or palladium, or ferromagnetic materials like permalloy or pure nickel. A combination of Ni and Pd for instance gives good electric connections while providing the necessary spin polarization. The second step of lithography finally defines large pads that can be used to connect the device to the measurement setup. With this method the gap between source and drain electrode can be as small as 10 – 15 nm. Larger gaps can also be produced (see Figure 1 where the typical layout of a chip and a scanning electron micrograph of a 46 nm junction is shown) and have a higher success rate (see Figure 2 for an overview of success rates). The most critical points in this process are the exposure and development of the nanojunctions. It might happen that short cuts between the electrodes occur due to an overexposure with the electron beam. However, we have optimized the parameters to minimize the spread of widths and thus maximize yield. Furthermore connections that are closed can then be used for electromigration to generate point contacts with gaps below anything achievable by pure lithography. Therefore the multi-contact samples with this spread of separations are ideal to provide the different widths as needed for the experiments.

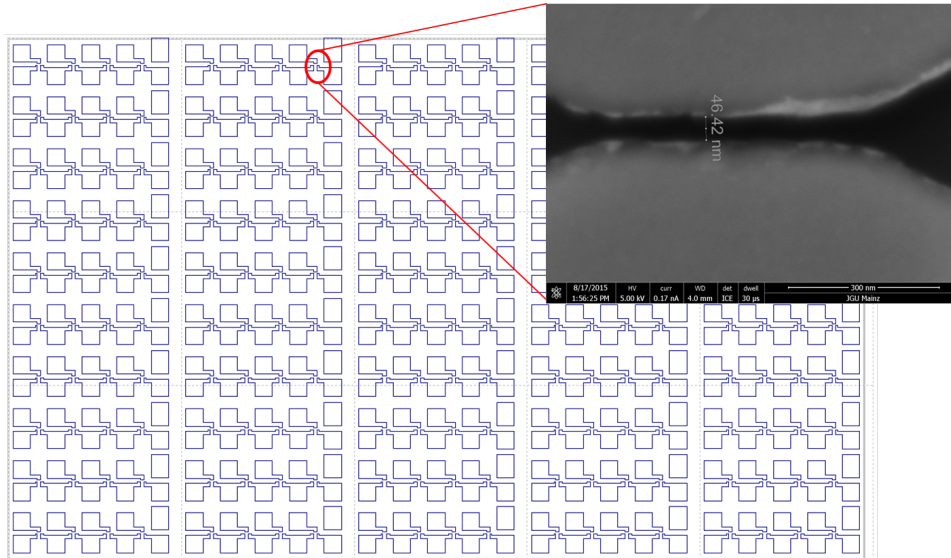


Figure 1: Typical layout of a chip with short-channel GNR FET-devices. In this case an array of $10 \times 5 \times 8 = 400$ junctions is shown. The inset shows a scanning electron micrograph of the gap between source and drain electrode with a spacing of 46 nm.

Electro-migrated nanojunctions

The electro-migration technique is a method to open nanosized gaps by moving material in a high electric current. The basic process is the same as for lithographically defined nanojunctions. The difference in this case is the intended very small connection between source and drain electrodes. Ideally, this connection has the form of a constriction, in order to maximize the current density at the point where the opening of the gap is planned. This is done by applying and increasing a voltage stepwise, while observing the resistance across the junction. Once the current is sufficient to open up a gap a feedback loop controls the voltage and shuts the process down at a certain threshold. Very small gaps below 10 nm can be achieved using this method. In general this process is less controllable and device loss can occur when the applied currents are too high.

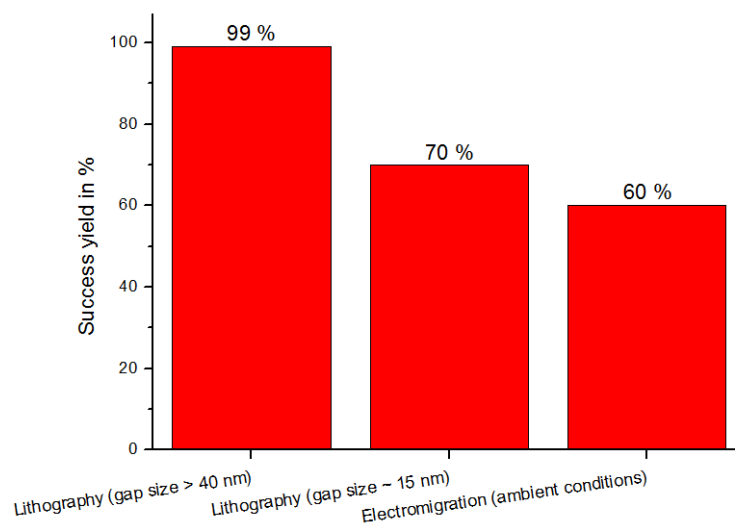


Figure 2: Success rates for metallic nanojunction fabrication.

Metal electrodes for contacting graphene nanoribbons

Graphene nanoribbons can be used as a channel medium which bridges the source and drain electrodes of the above described nanojunctions. As there are different ways to produce well-defined graphene nanoribbons in chemical bottom-up synthesis processes, there are also different approaches to fabricate a device. For solution-synthesized GNRs the method of choice is to fabricate the electrodes first as described. Subsequently the GNRs which are in a solution are simply drop cast on top of the electrodes. The critical problem is that the hydrophobic GNRs are agglomerating instead of forming a thin film on the surface of the substrate. This impedes the device production since the nanoribbons do not lie flat across the nanojunction, but form bundles at isolated positions on the substrate. To overcome this problem the SiO₂ surfaces were functionalized with alkyl chains by treatment with corresponding alkyl silane reagents. However, the electric measurements on such functionalized surfaces turned out to be challenging and disadvantageous presumably because the GNRs were wrapped in the insulating alkyl chains. Therefore, JGU and CNR-NANO partners are developing other deposition methods without the alkyl functionalization such as a use of graphene electrodes and mechanical transfer of a GNR film prepared on a membrane filter.

In the case of GNRs grown in a chemical vapour deposition (CVD) process, they are firstly brought onto the silicon/silicon dioxide substrate. The electrodes are afterwards patterned on top of the thin film of nanoribbons. Using this approach devices where GNRs bridge the junction are found more often compared to the case of solution-synthesized GNRs. On a chip as shown in Figure 1 with 400 junctions around 5 working devices can typically be found, which corresponds to yield of 1.25% (Figure 3).

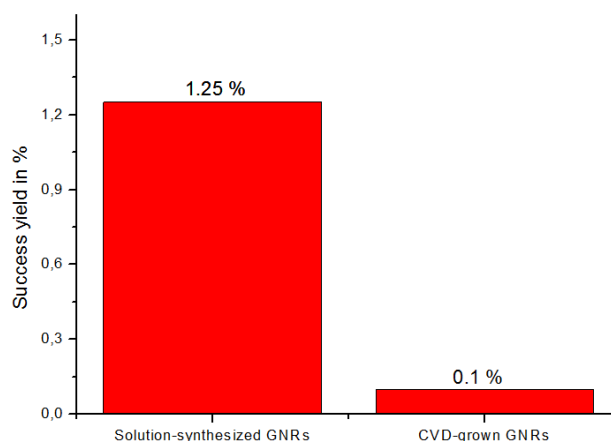


Figure 3: Success rates for GNR-FET device production using metallic nanojunctions.

Finding that graphene nanoribbon react very sensitively to environmental influences, we intend to minimize contaminations which come along with electron beam lithography necessarily. Such contaminations are the effect of resist residues (PMMA), damages by the electron beam and contaminations due to the exposure to solvents involved in the process. Additionally heating steps might also lead to damages. This leads to the idea to fabricate electrodes without the need of lithography. Shadow-mask evaporation, where a solid metal-mask defines the area on a chip where the metal contacts shall be, are a way to reach that goal. The advantage here is that no further resist or solvent touches the graphene nanoribbons on a silicon/silicon dioxide substrate. The disadvantage however is, that only larger channels can be defined (in the order of 10 μm). That means that there is no chance to measure electric transport through a single graphene nanoribbon. Instead, there will always be a network of ribbons, which form a conducting path. Here, interface resistances are not well-defined and may vary strongly from device to device. The rate of finding a device, where a finite conductance can be measured is nevertheless remarkably higher than compared to the lithographically processed devices. Using this route to fabricate devices, we a significantly higher number of working devices on a chip. Here, we find approximately 25% of working devices for chevron-white book

type ribbons as well as for armchair ribbons ($N=7$ and $N=9$). Heteroatom-doped graphene nanoribbons exhibit more defect centers and are not as laterally extended as the undoped ribbons. Chips with these ribbons tend to have a lower yield of working devices with up to 10%. Figure 4 shows a devices with a $10\ \mu\text{m}$ gap defined by shadow-mask evaporation of gold.

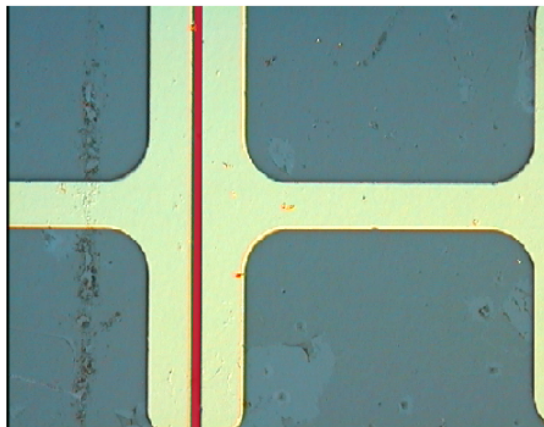


Figure 4: Optical micrograph of a graphene nanoribbon FET-device, defined by shadow-mask evaporation of gold (yellow). The gold electrodes are surrounded by a monolayer film of graphene nanoribbons. The active GNR-FET-Channel is shown in red.

Non-local spin valves on epitaxial graphene

Non-local spin valve devices are fabricated in a 4-step lithography process on epitaxial graphene on the C-face of silicon carbide (SiC). In the first step, we define the metal contacts on graphene. In order to keep the contact resistance as low as possible, this is performed as the first step to prevent the exposure of graphene to other step of lithography that could lead to a degradation of its quality. The second step is the patterning of graphene channels. After the growth of graphene, it is present everywhere on the SiC-substrate. As we need defined conducting channels, we prepare an etch mask by lithography. Then, the channels are etched using reactive oxygen plasma etching. The third step is the realization of the larger parts of the electrodes. These include also the large pads to give the possibility to contact the device afterwards using conducting needles of a probe station or a wire-bonding technique. The final fourth step is the patterning of ferromagnetic electrodes. All the previous steps including the electron beam lithography necessary for this last step is carried out by CNR-NANO. The evaporation of the ferromagnetic material is done JGU-MAINZ. Figure 5 shows in image of a complete device.

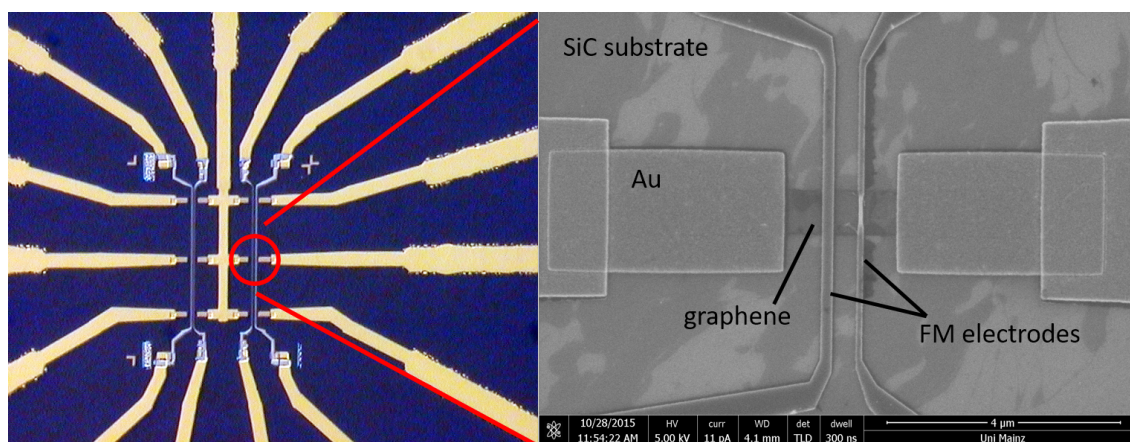


Figure 5: Example of a graphene device with ferromagnetic electrodes. On the left a complete device with 6 graphene junctions is shown. Usually, on a whole chip, 16 of these devices are made. On the right it presented a zoom of an individual junction. The graphene channel, the ferromagnetic electrode and the gold contacts are indicated.

In the following we report the statistic related to the devices fabricated so far. The activity started from the second year of MoQuaS and after the first samples used to optimize the device geometry and the ferromagnetic metal growing conditions the ultimate samples are currently under measurements.

Statistics on the 4 chips fabricated so far:

Chip 1:

Design – 12 devices

Successful lithography & metal evaporation: 9 devices

Electrical characterization: High contact resistances/partially missing graphene. 1 device found where 3 contacts made

Hanle measurement possible. No significant non-local spin resistance signals were observed.

Chip 2:

Design: 72 devices

Successful lithography & metal evaporation: 39

Electrical characterization: Devices show shortcuts, possibly due to conductive substrate. No non-local spin resistance could thus be measured.

Chip 3:

Design: 96 devices

Successful lithography & metal evaporation: 78

Electrical characterization: *ongoing*.

Chip 4:

Design: 96 devices

Successful lithography & metal evaporation: 69

Electrical characterization: *ongoing*.

Graphene-based Molecular Electrodes (or nanojunctions)

In the following, we report the fabrication procedures and yields of graphene-based electrodes. Here a graphene channel is used as a “bridge” electrode to connect molecules to massive metallic contacts. The use of graphene as an electrode, with its intrinsic two-dimensional nature and the possibility to exploit carbon-bonds, is expected to improve the affinity with the molecular units.

All the devices we fabricated consist on a graphene channel contacted with metal electrodes and patterned to obtain a physical gap which shall be bridged by the molecular compound of which we want to study the electrical properties. Concerning the type of graphene materials we have used, since the start of MoQuaS we have employed exfoliated graphene and graphene epitaxially grown on the C-face of SiC; since the third year of MoQuaS we also started to fabricate and utilize devices made with single layer graphene grown by chemical vapour deposition (cvd) on Cu and transferred on substrates made of 300 nm of SiO₂ over doped Si that can be employed as a backgate. The reason to test different type of graphene is described in the following. Exfoliated graphene is the highest quality graphene available to date, however its small size usually result in a small number of available device. We used graphene on SiC as a source of large area graphene for the rapid integration of a large number of device for our molecular compound. The final test on cvd-graphene transferred on SiO₂ are motivated by few advantages of this material with respect to graphene on SiC. In particular the possibility to use a common backgate for the device is expected to lead to a consistent increase of the number of available device. In addition the large gate tunability of single-layer graphene on SiO₂ can be an additional resources that could be exploited for some devices.

For all of the studied devices, the first fabrication step is to obtain electrical contact onto graphene. Secondly, the graphene channel is patterned in order to obtain a gap and finally the molecular unit is deposited on the device and measured. We will now consider all the fabrication steps individually and consider the different results obtained for the different type of graphene.

Fabrication of graphene-based electrical contacts.

The first fabrication step, common to all devices, is the fabrication of metal contacts on graphene. The contacts are obtained by electron-beam lithography (EBL) and metal evaporation. The procedure is slightly different regarding the exfoliated and the large area (epitaxial or cvd) graphene. Here we will consider the total amount of contact realized, regardless of the specific type of device.

Fabrication of metal contacts on exfoliated graphene

Graphene flakes are obtained by the standard so called “mechanical exfoliation” technique using adhesive tape and high-quality graphite ores. Suitable flakes are located by optical microscopy and then the contacts are made by EBL. This is a rather time consuming technique, as a specific pattern has to be prepared for any individual flake. However, once the electron exposure dose is optimized, the only source of failure is represented by human errors (lithography misalignment, sample damages, etc...) or by a non perfect lift-off of the evaporated metal. There is also the possibility that some graphene flakes are not stable, folding or detaching from the substrate during the fabrication. Also some inhomogeneity on the flakes (not visible under the optical microscope) may results in poor electrical contacts. Since the start of MoQuaS project, we fabricated 418 pairs of electrical contacts, finding low resistances ($\leq 1\text{K}\Omega$) and ohmic behavior in 371 of those, which is a success rate of the order of 90%.

Fabrication of metal contacts on large area graphene

Large area graphene (graphene on C-face of SiC and cvd-graphene transferred on SiO₂) grows on the whole surface of the substrate, which can be from few mm squared to wafer scale. In order to realize electrical devices, it is therefore necessary to pattern the graphene with the desired geometry. This is obtained with an additional lithography process,

consisting in a EBL pattern an oxygen plasma etching, while the metallization is realized in an identical manner as presented in the previous section. The additional fabrication step induces more sources of failure (lithography misalignment, non-perfect etching etc...), in addition the graphene may not be perfectly homogeneous through the whole sample, resulting in low quality devices. Moreover, for the case of cvd-graphene, the necessary transfer step is an additional source of possible failure (the samples can break or fold in some parts). The final result is that the yield of successful electrical contacts is somehow lower than for the exfoliated graphene (595 out of 776 for graphene grown on the C-face of SiC and 96 out of 130 for the cvd-graphene transferred on SiO). However, as in a single fabrication step several tens of devices can be realized in parallel, this method results to be more time-efficient than the previous one.

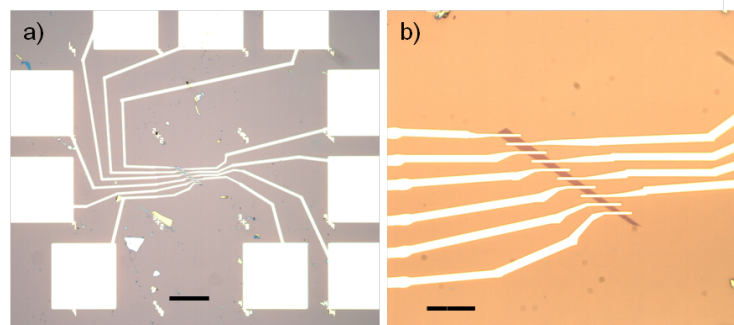


Figure 6: (a,b) optical microscope images of a graphene flake after contacts fabrication. Scale bars are 100 μm (a) and 10 μm (b), respectively.

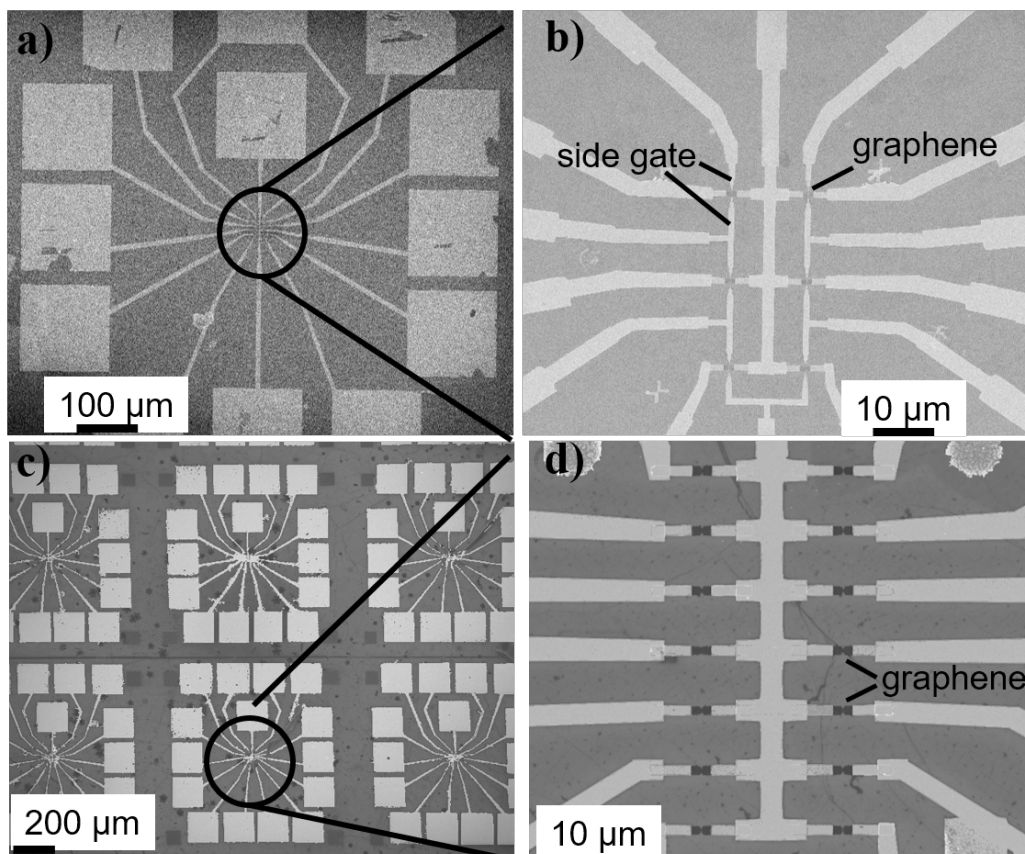


Figure 7: (a-d) Electron microscope images of typical examples of large area graphene devices. Epitaxial graphene grown on the C-face of SiC is shown in a,b) while the devices realized on cvd-graphene transferred on SiO₂ are shown in c,d). It is interesting to note that for the case of graphene/SiO₂ system it is possible to realize a significantly higher number of junctions, due to the possibility to exploit a backgate.

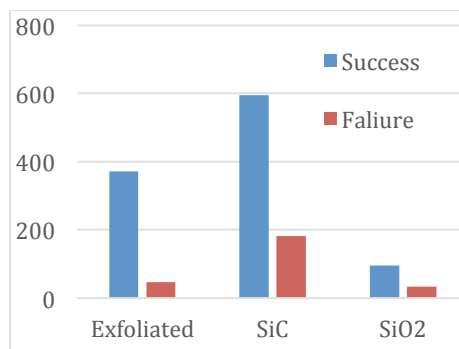


Figure 8: Total yield of success for metal contacts on different type of graphene

Fabrication of a physical gap in graphene

After having fabricated the graphene devices described in the previous section, the subsequent fabrication step is to create a physical gap in the graphene channel, which will eventually be bridged by the molecular compound under study. The final size of the gap is therefore related to the actual size of the system under investigation, and different techniques are employed in order to obtain gaps of different sizes as the compounds of interest for our project can be an individual molecule (around 1 nm in size) or even graphene nanoribbons (GNRs) which can be long several tens of nanometers.

Gap fabrication by lithography

The most straightforward approach to create a gap in the graphene channel is to employ electron beam lithography and oxygen plasma etching. In this way, gaps in the order of 50-200 nm can be easily obtained. Such gaps can be in principle used to contact solution-synthesized GNRs which can be as long as hundreds of nanometers or thin film of transferred cvd-grown GNRs. An advantage of this technique is that it can be performed during the same patterning step in which the graphene channel are fabricated as described in the previous section. The main source of error which is left here is that the patterning parameters (in particular exposure dose and etching time) are optimized on “average” sample. Therefore, as the large area graphene can have some inhomogeneity through the whole sample surface, the same etching parameters can result in under-etching when the graphene is thicker than average and in over-etching when the graphene is thinner than average. To verify the actual realization of a gap in the channel we use two main criteria. Firstly, no current must be measured in the device before the molecular deposition; secondly, the success of the lithography process is monitored by an inspection with an electronic microscope (SEM). We have fully analyzed (I-V measurements and SEM imaging) more than 150 junctions on graphene on SiC and transferred on SiO₂ with a success rate usually above 80%. From this count we excluded a particular sample, on which we have tried to obtain a gap size as small as possible by using an exposure dose 20% lower than usual, where the success rate dropped to 50% on a total of 72 devices. Because of this poor success rate, to which did not correspond a significant improvement in the final gap size, this procedure was never replicated.

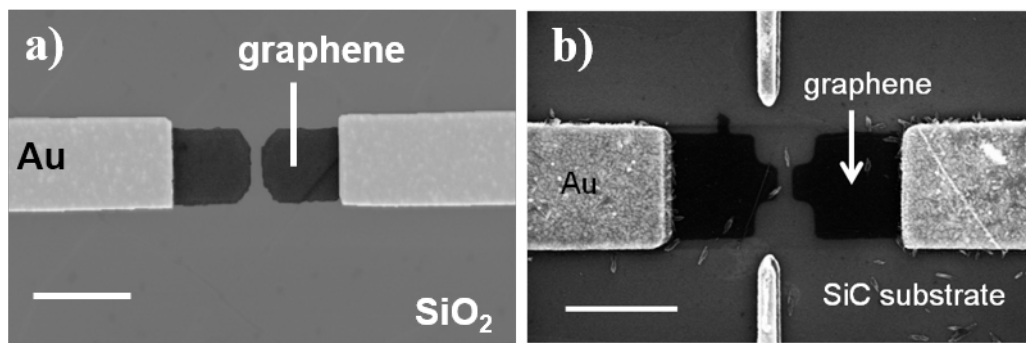


Figure 9: a),b) Electron microscope image of a graphene device with gap defined by lithography on SiO₂ (a) and SiC (b). The scale bars are 1 μm, the gap size are ~ 100 nm.

Gap fabrication by the electroburning technique

Gaps in the range 1nm – 50nm can be obtained by the electroburning technique. This consists in applying a voltage ramp to the channel and rapidly stopping it when the at the high temperatures reached by the Joule heating the carbon atoms react with oxygen leading to a break in the device which can be visualized during the measurements as an abrupt increase of the resistance.

Feedback-controlled electroburning for nanometer sized gaps

When the electroburning procedure is performed with the help of a computer-controlled feedback loop and interrupted immediately after the process has begun (and in some cases repeated until a certain low-bias resistance is reached) gaps of few nanometers in sizes can be obtained. In principle, they can be suitable to contact individual molecular units. The success criterion for the procedure is usually considered the observation of a tunneling current at low bias voltages (below 2 V), which, according to the most used models for the tunneling current through a vacuum gap, corresponds to a gap size below 5 nm. On the other hand, the procedure can fail because the sample cannot be completely electroburnt (in this case a linear I-V curve is still measured after the process) or because the feedback is not fast enough to stop the process and the device opens completely, leading to a gap wider than 5-10 nanometers and no tunneling current is measured between -2V and 2V. When working with exfoliated graphene flakes, we have demonstrated that the yield of success can be improved by working under vacuum: 20 devices out of the 58 processed in air vs 33 devices out of the 57 junctions processed in vacuum showed a tunneling current after the electroburning, while the percentage of the devices impossible to electroburn remained almost constant at around 25%.

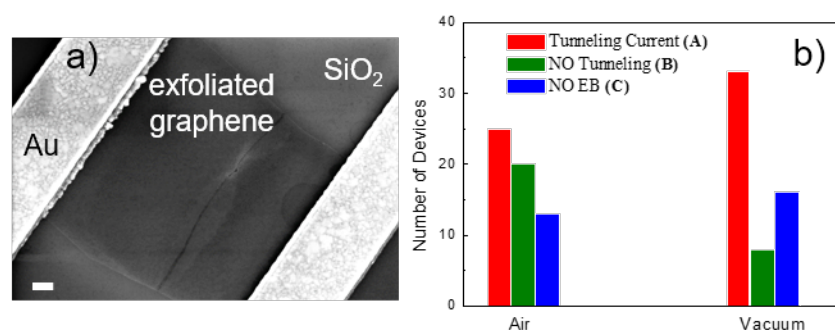


Figure 10: Electron microscope image of a gap obtained by controlled electroburning on exfoliated graphene (a) The scale bar is 300 nm. b) yield of success of the electroburning technique as described in the text in air and in vacuum for the exfoliated graphene devices. Devices marked with (A) showed a sizeable tunneling current at low biases after the electroburning, which is a signature of the formation of a gap in the nanometer range. Devices indicated as (B) showed no detectable current, probably indicating a larger gap or even the complete breaking of the device. Finally for the

devices marked as (C) it was not possible to perform the electroburning, probably because the original flakes were too thick.

Since the success rate for single molecule devices is expected to be extremely low, we developed the electroburning procedure also for large area graphene, namely graphene epitaxially grown on the C-face of SiC and graphene grown by cvd and transferred on SiO₂. We have already reported in the previous section the yield of successful contacts on large area graphene samples. For these particular devices, devoted to the study of single molecule junctions, we make also side gate contact as close as possible to the junction. This adds an additional possible failure in the device, that is a shortcut with the gate. This is usually checked before the electroburning and defected devices will not be proceeded further. For graphene on SiC devices we found 104 usable devices out of the 133 obtained from the fabrication procedure. For graphene on SiO₂ we found 48 usable devices out of the 58 fabricated with success.

When working on the epitaxial graphene, the electroburning procedure is not working in vacuum, therefore we processed our devices only in air. Initially, we performed the electroburning procedure until the observation of a tunneling current compatible with the opening of a gap of few nanometers in size at room temperature. We worked on 36 devices, finding a tunneling current in 21 of those. However, no current was ever observed at low temperature ($T < 4K$) where the electrical measurements of the molecular devices are done. Therefore for the fabrication of the graphene contacts for individual molecules we proceed in the following way: firstly the graphene channel is thinned with a controlled electroburning sequence until a resistance on the order of $10^3 - 10^6$ Ohm is reached (the I-V curves still linear in this regime). Then the molecules are deposited as it will be described in the next sessions and the sample cooled.

In a first set of measurements, we processed 20 devices and in 9 we have been able to control the final resistance of the junctions, while in the remaining the process was simply not fast enough to stop leading to an opening of a gap in the channel. After cooling, all of the 9 devices showed a measurable currents at low voltage, compatible with either a gap of few nanometers or a small object trapped between the electrodes (we refer to the next sessions on how to check the actual origin of this current). That signified a success rate lower than 50%. After an optimization of the response time of the feedback software, we have been able to consistently increase the final yield. With the improved software we have processed so far 84 junctions being able to achieve a controlled final state for 72 (85.7%) of those. When measured at low temperatures, we found a sizeable current in 61 (72%) junctions, that signifies an increase of the yield of devices working at low temperature from less than 50% to more than 70%.

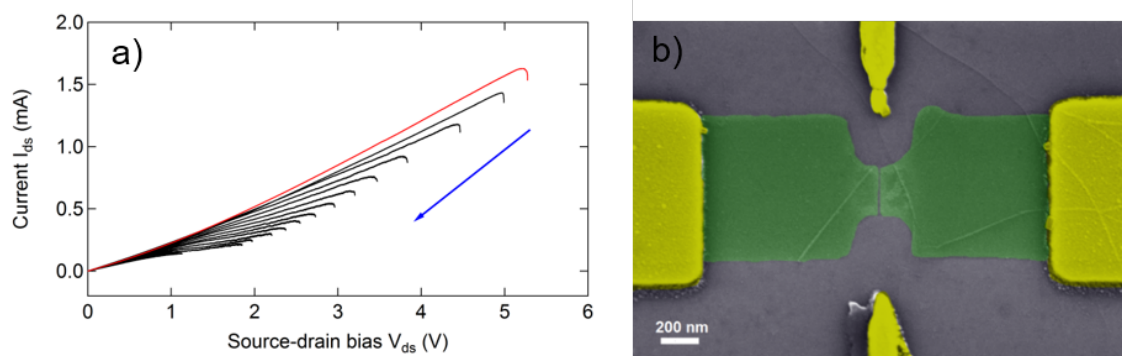


Figure 11: a) Set of I-V characteristics showing the evolution (see blue arrow) of the feedback-controlled EB process. A voltage ramp is applied across the device until its resistance increases by more than a predefined percentage. The process is iterated until the low-bias resistance reaches $100\text{ k}\Omega - 4\text{ M}\Omega$. b) False colour SEM image of a graphene junction after EB: a gap is visible in the centre of the middle “notched” region of the device.

During the last year of MoQuaS, we started also to fabricate devices on cvd-graphene transferred on SiO₂. Some of the advantages of this type of graphene include the possible use of the back gate as an additional tuning for the devices. The yield of success of the room-temperature electroburning for this type of graphene is similar to what we found for graphene on SiC. We found a low temperature signal in 8 devices from the total of 12 we processed. However, one of the most appealing possibilities offered by the use of the cvd-graphene is to perform the electroburning in vacuum and

even at low temperature, directly in the cryostat, that is expected to lead to more controlled and clean samples. In this case, we deposit the molecular compound before cooling and then do the electroburning directly before the measurements, that is what is usually done also for metal electromigrated junctions for single molecule transistors. The low temperature electroburning turned out to be more critical to control and so far we have obtained a successful electroburning on 10 devices over a total of 21 (< 50%). We note that the results on the cvd-graphene devices are still in progress. With realistic optimization in the process (for instance by reducing the speed at which the electroburning is performed) we expect to achieve final yields similar to what is found on epitaxial graphene. The important advantage here will be to have a more clean sample since the opening of the molecular gap is performed already at low temperature, in vacuum and just before the measurements. The possibility to fill the gap with unknown impurities will be therefore significantly reduced.

Non-controlled electroburning for large gaps

The gaps obtained by the technique described previously can be as small as few nanometers; however they are often not stable under high electrical bias (> 0.5V). Such bias values are usually needed for the measurements of the GNRs electrical properties, as they usually show high contact resistances. In order to overcome this limitation, we also employ the same electroburning technique removing the fast feedback loop in order to stop the process when the channel is already completely open. This creates gaps with sizes as small as 10nm, which are usually stable even when biased at voltages as high as 2V or more and can thus be used to contact GNRs. The success criterion for this procedure is thus to not observe any tunneling current after the electroburning sequence. In analogy to what presented before, a source of failure is again represented by junctions that cannot be open completely, even after the repetition of several electroburning cycles. In addition, the process can be so fast that the channel is removed completely, leading to gaps larger than hundreds of nanometers or even the melting of the metallic contacts. Such failure can be visualized with an optical microscope before the GNR deposition. The technique was employed on different type of graphene, with a generally high success yield. We obtained a gap suitable for GNR deposition on 115 exfoliated graphene devices over 214 (54%); 79 graphene on SiC device over 96 (82%); 42 cvd-graphene device over 49 (86%). The higher rate of success found in large area graphene devices is ascribed to the use of more uniform graphene samples, significantly lowering the number of devices where the electroburning was not possible to achieve.

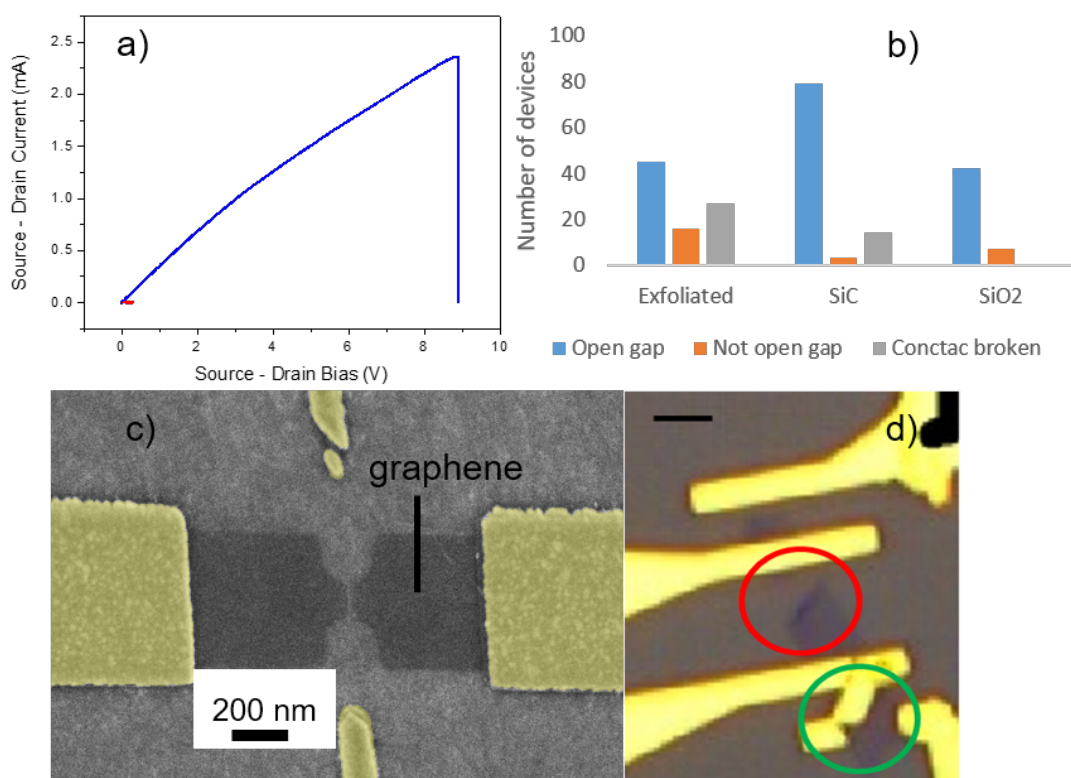


Figure 12: a) Typical current-voltage measurements for a non-controlled electroburning. The voltage ramp is stop only when the device has already reached the high resistance state. b) Yield of success for the process on different graphene devices. The blue represent the number of devices with a gap suitable for contacting GNRs. In orange are shown the device where the electroburning did not lead to an opening of a gap in the channel. In grey it is reported the number of devices where the electroburning leads to a completely broken device, similar to the ones shown in d). c) SEM image of a typical gap obtained by the non-controlled electroburning on a graphene on SiC device. The gap size is in the range 10-20 nm. d) Optical image of an example of an exfoliated graphene device broken by the non-controlled electroburning. The red circle underlines the region where the graphene flake is folded, leaving a gap of several hundreds of nanometers. In the green circle a broken golden electrode is shown. The scale bar is 1 μm .

Deposition of the molecular compounds on the graphene devices

The final step of the fabrication of graphene-based molecular devices consist in the deposition of the molecular compounds on the devices fabricated according to the methods described in the previous sections. The final goal is indeed to address the properties of the molecular systems (in particular charge and spin degrees of freedom) by measuring the electrical current in the devices. The systems studied with the graphene devices in the MoQuaS project are molecular magnets of the TbPc families and atomic-precise graphene nanoribbons (GNRs). We will now describe the different procedures employed to deposit the compounds and the different criteria used to validate their actual presence on the devices and therefore to establish the final yield of success of the molecular assembly.

The total number of devices analyzed in the following sections corresponds roughly to the total number of devices fabricated as described previously. Indeed, additional sources of failure may occur, such as accidents on the sample (for instance a sudden gate leakage may break the sample under measurements but also few samples close to it), degradation (due to the limited number of devices that can be measured simultaneously, some samples are cooled and

re-heated several times before being measured), additional electrical breaking during the micro-bonding. This translates in an additional loss usually of the order of 10% of the available devices at this point. This issue is particularly critical for the single molecule devices fabricated with the epitaxial graphene on SiC. For these particular samples the graphene junctions can be cooled down and heated up several times before the final measurements, increasing the loss at this point to 20%

Deposition of Magnetic Molecules

We adopted two slightly different procedures for the molecule deposition and we will address them separately. TbPc₁ molecules are firstly dispersed in a dichloromethane solution which is then dropcasted onto the epitaxial graphene devices described previously (i.e. after a preliminary not-complete electroburning step). After the deposition, the electrical behavior of the devices is not changed. The system is then cooled to low temperature (< 100 mK) and measured.

For the Tb₂Pc₃ molecule-devices, we mainly employed the low temperature electroburning with cvd-graphene transferred on SiO₂, as described previously. In this case, the molecular solution is dropcasted on the intact devices and then cooled down directly to low temperature (< 100 mK). At this point we performed the electroburning with the yield described in the previous section and then the device is measured.

In order to establish the presence of a magnetic molecule of the TbPc₂ or Tb₂Pc₃ families the procedure is similar and the following criteria have to be fulfilled: a) measure a current at low bias voltages. This assures that the gap is not too big or empty. b) the current must be gate-dependent showing the typical feature of Coulomb blockade phenomena usually associated to electrical transport through a molecular unit. The need to measure a gate dependence introduces another possible source of failure that is gate leakage. While in principle this error results from the lithography process and it has been already addressed, other sources of leakage may happen only at low temperature and therefore they can be verified only at this step of late electrical characterization. This check assures that “something” actually fills the gap of the graphene electrodes although at this point it is not yet possible to distinguish between a magnetic molecule and other nano-sized object (small impurities, graphene residual left after the electromigration, broken molecules or parts of it). c) the magnetoconductance of the device must reflect the magnetic properties of the TbPc₂ molecules, well known as measured on bulk. These properties include a strongly anisotropic magnetic hysteresis and spin flip transition at specific field values corresponding to the nuclear spin moment of the Tb ion. This last step is the final check that an intact TbPc₁ molecule is actually the system under investigation.

Concerning the TbPc₂ molecules, 70 devices from the processed 104 ones have reached this step as described previously. We observed Coulomb blockade phenomena for 12 devices, while in the other 58 we found no gate dependence; we note that it was not possible to verify the gate dependence on 21 devices because of leakages. Finally, these remaining 12 devices have been measured under magnetic field, finding an anisotropic hysteretic signal in 2 of them, one of the fingerprints of the TbPc₂ molecules. However, it was not possible to assess the nuclear spin of the Tb ion in none of these samples. The reason was that the system was not stable enough for completing the necessary characterization. Also the presence of damaged molecules or even too many molecules close to the gap can be a source of disorder as they all contribute with some magnetic signal averaging out the response from the individual units. Regarding the Tb₂Pc₃ triple decker, we have so far cooled down 21 devices and 10 passed the low-temperature electroburning as described previously. We found a gate dependent signal on 5 devices and no dependence on the other 5 (on 2 we found a gate leakage). So far no magnetic signal is still detected.

It is worth to comment about the poor yield of Coulomb blockade signal found for the TbPc₂ devices, where we employed the epitaxial graphene. This is to be ascribed to a large set of samples where we have verified, after the measurements, that the side gate were badly coupled to the devices, as a consequence of a systematic fabrication

error. Without this issue, the general yield of Coulomb blockade phenomena is around 40%, similar to what is found for the Tb_2Pc_3 molecules, where we employed cvd graphene transferred on SiO_2 .

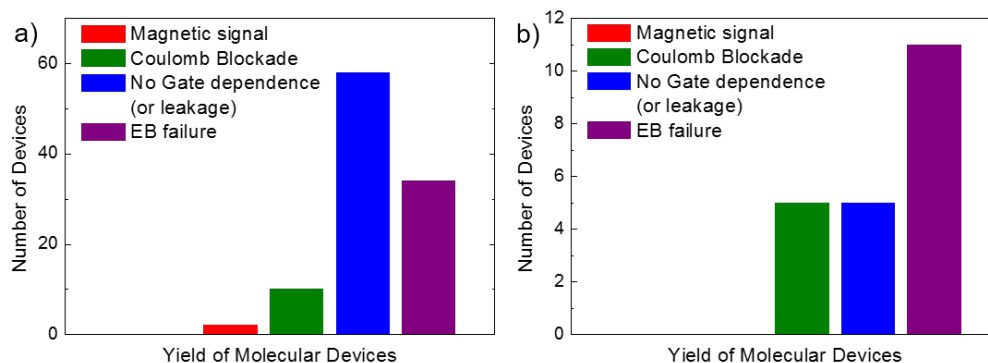


Figure 13: a) Yield for the $TbPc$ single molecule devices. From the total of 104 devices processed, 70 survived the partial electroburning to show a sizeable current at low temperature (the purple column showing the broken devices). For 58 of those (blue column) it was not possible to continue the measurements since the gate was found to leak or to have no effect on the current, while the remaining 12 displayed a gate-tunable current and the onset of Coulomb Blockade (red and green columns). 2 of them (red column) also showed an anisotropic magneto-conductance which is one of the fingerprint that the current is probing a $TbPc$ molecules. b) same as a) for the Tb_2Pc_3 molecules, processed with the low-temperature electroburning. From a total of 21 devices, 10 survived the electroburning and 5 of them showed Coulomb blockade behavior. No magnetic signal was detected so far due to the limited number of processed sample.

Deposition of graphene nanoribbons.

Also atomic-precise graphene nanoribbons have been deposited on the graphene-based devices described in the previous sections. Since these systems are relatively recent, their electrical transport properties remain to be fully characterized. The first step is therefore to characterize their field-effect transistor behavior, even in the form of a thin film. Indeed, the first indication that one or few nanoribbons connect the graphene electrodes is the observation of current in the junction (we deposit the GNR only on completely open gaps displaying no measurable current in the range of -2 V to $+2$ V). Secondly, we look for a gate dependence of the current, in particular a field effect transistor behavior compatible with the large-gap semiconductor nature of the GNRs. As already pointed out for the magnetic molecules, a gate leakage is therefore an additional source of possible failure. This is a critical issue especially for the devices made with epitaxial graphene on SiC. Indeed, on these devices the electric field tunability is performed with lateral side gates, since it is not possible to use a backgate. The side gates have to be rather close to the device channel, otherwise their effect will be negligible. The deposition of GNRs can therefore shortcut the graphene channel of the device with the lateral gates. This issue is expected to be largely removed by using the devices made with cvd-graphene and transferred on SiO_2 . As the GNRs can be produced by different approaches, we also employed different strategies to deposit them on the graphene channels.

Deposition of solution-synthesized graphene nanoribbon.

Solution-synthesized GNRs are firstly dispersed in solution from powder and then drop cast on the graphene devices fabricated using the not-controlled electroburning, with gap sizes in the range of 10-20 nm. We chose these devices as the ribbons tend to agglomerate and roll up on the surface during the deposition and even if they can be as long as

several hundreds of nanometers, it is very unlikely that a ribbon can bridge a gap larger than 50-100 nm which is the smallest sizes we can obtain by lithography.

From the 70 open gaps produced as described in previous section we found the appearance of an I-V curve in 14 junctions. In some of them (5) we found current in the tens of μA range, and a small gate dependence. This signature is compatible with the signal expected from bundles of GNRs. In the remaining 9 junctions we found currents in the order of few nA at 1V of bias. While these values can be related to one or few ribbons bridging the gap we never observe any gate dependence, at least at room temperature. Also the signal appeared to be quite unstable, changing over the time scales of the measurements (days or weeks). The samples were also cooled at low temperature, finding a measurable current below 100 K in 2 junctions, one of which also showed a gate dependence at 2 K.

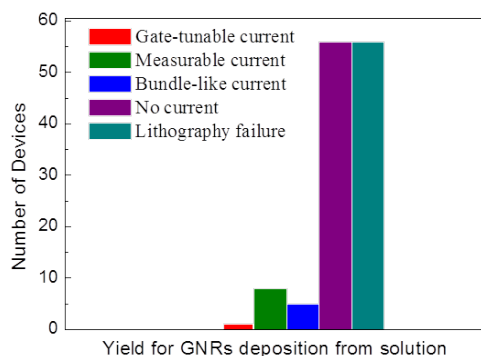


Figure 14: Yield for the deposition of solution-processable GNRs on graphene electrodes. From the total of 126 processed devices, 56 (cyan column) were lost during the fabrication (see also section 2.2.2). No signal was found on 56 devices (purple column) of the remaining. 5 devices showed a signal compatible with GNRs bundles or aggregates (blue column). Finally, 8 devices showed a measurable current compatible with one or few ribbon bridging the gap (green column) and 1 device displayed a gate-tunable current (red column), although only at low temperature.

Deposition of solution-synthesized graphene nanoribbon by electrospray technique

In a recent set of experiments, we employed the electrospray deposition (ESD) technique to deposit solution-processable GNR also onto graphene electrodes for the realization of three-terminal devices. The ESD seems particularly appealing since the combination of high voltages and temperatures permits to spray onto any type of substrate even heavy molecules such as the GNRs with the possibilities to obtain isolated units. We have described the related procedure and results in the scientific report, here we will analyze only the yield of the results, with particular regard to the comparison with the drop casting method described previously.

We employed the same type of graphene device as for the dropcasting method. We realized 15 open gap with the non-controlled electroburning on exfoliated graphene device. After the ES-deposition, a measurable source-drain current was present on 4 devices (we applied a bias potential not higher than 1 V). Interestingly, we did not observe the signal associated with GNR bundles and moreover for two devices we detected a significant gate dependence, with a field effect transistor effect with current on/off ratio as high as 5 already at room temperature. While the statistic on ESD devices is still to be improved, these first results are very encouraging and show the potentialities of the ES technique to deposit GNR suitable for the device fabrication.

Deposition of cvd-grown graphene nanoribbon.

Atomic precise GNRs can also be grown by chemical vapour deposition (cvd) method on a metallic substrate (see the scientific report for more details). The GNRs grow forming a continuous layer that can then be detached from the metal and deposited on an arbitrary substrate, such as a pre-patterned graphene electrodes array. The GNR film is roughly as large as the metal substrate, that can be up to several cm² in size. In order to maximize the number of total devices, we

used electrodes made with large area graphene: since we expect that the ribbons film can connect even large gaps, we used devices with gap obtained by lithography (gap size \sim 100-200 nm) and also devices with gap induced by the non-controlled electroburning (gap size 10-20 nm). The following statistic is related only to devices made by epitaxial graphene on SiC, since the measurements on the cvd-graphene electrodes are still undergoing. As already said, we expect with this material a significant increase of the total number of working devices.

As a first step, we prepared a layer of GNRs on the metal and then transferred it to the graphene electrodes. In a first attempt the metal removal was performed directly with the GNRs film in contact with the graphene devices. However, it turned out that the etching solution was detrimental also for the electrodes fabricated on the graphene and no devices could be measured after the process. Therefore, we now perform the transfer adding a supplementary transfer step with the aid of a sacrificial layer of polymer (such as PMMA) even if its use can worsen the final properties of the GNRs.

We employed so far two types of GNRs: the first measurements were performed with chevron-type GNRs, while more recently we started the characterization of armchair GNR with width equal to 9 lines of Carbon (9-AGNR). This novel type of GNR are expected to have better electrical quality than the previous one (see the scientific report for more details). We will address them separately.

The chevron-GNR have been transferred on a total of 157 open graphene gaps. We found a measurable current in 25 junctions, and a significant gate dependence in 5, compatible with the GNRs expected properties, while in the remaining either no gate dependence or a gate leakage was observed. For 4 devices it was even possible to measure a sizeable photocurrent. By analyzing the photocurrent dependence on the photon wavelength we derived the GNR bandgap that was found to be perfectly in agreement with what directly measured by absorption experiments on thick film samples of GNRs.

When comparing the results obtained for cvd-grown and the solution-processable GNRs it is important to point out that for the cvd-grown GNRs we found a strong gate dependence (up to 10^4 for one sample) even at room temperature and that the electrical signals were found to be extremely stable, lasting almost without any variations through timescales of several months. We therefore come to the conclusion that GNRs grown by the surface-assisted methods (such as the cvd) are more suited to be integrated in electrical devices. Therefore, in order to improve the performances of GNR-based devices, we started the production and characterization of GNR/graphene devices with 9-AGNR as the channel. We have so far deposited the 9-AGNR on 87 empty graphene gap and found a sizeable current on 25 devices. We found a gate leakage on 16 devices (probably caused by shortcut between the side gate and the graphene channel induced by the GNR film) and a sizeable gate dependence on 3 devices of the remaining 9. The results are summarized in Figure 15, where the increase of the yield of success between the two types of GNRs is clearly visible. In particular, the devices made with the 9-AGNR consistently show higher currents than the ones with the chevron-GNRs. We will therefore concentrate on this novel type of GNR for making electrical devices.

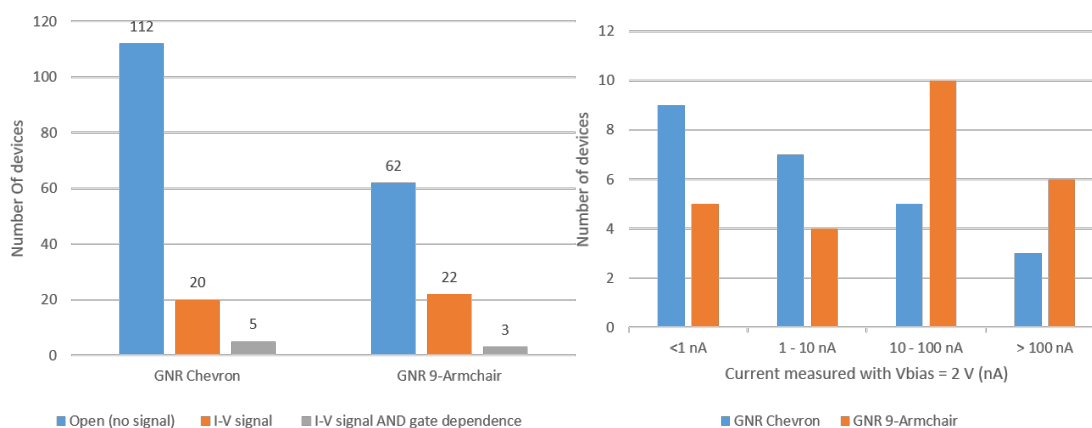


Figure 15: Left: total yield for the transferred cvd-grown GNRs with a comparison between GNR/graphene devices using chevron type GNR and the newly synthesized 9-AGNR. The total number of devices with and without a current signal on the I-V is shown for the two type of GNRs. Right: number of devices showing a current (measured at 2 V) in a

specific range for the two GNR type. It is found that the device with 9-AGNR usually have higher on-state current values.